Dynamics of liquid ^{4}He in confined geometries from time-dependent density functional calculations

Luigi Giacomazzi, Flavio Toigo, and Francesco Ancilotto
Istituto Nazionale per la Fisica della Materia and Dipartimento di Fisica "G. Galilei," via Marzolo 8, I-35131 Padova, Italy
(Received 17 October 2002; published 3 March 2003)

We present numerical results obtained from time-dependent density functional calculations of the dynamics of liquid ^{4}He in different environments characterized by geometrical confinement. The time-dependent density profile and velocity field of ^{4}He are obtained by means of direct numerical integration of the nonlinear Schrödinger equation associated with a phenomenological energy functional which describes accurately both the static and dynamic properties of bulk liquid ^{4}He. Our implementation allows for a general solution in three dimensions (i.e., no symmetries are assumed in order to simplify the calculations). We apply our method to study the real-time dynamics of pure and alkali-doped clusters, of a monolayer film on a weakly attractive surface and a nanodroplet spreading on a solid surface.

DOI: 10.1103/PhysRevB.67.104501 PACS number(s): 67.70.+n, 67.40.Bz, 68.08.Bc

I. INTRODUCTION

Density functional (DF) methods[1] have become increasingly popular in recent years as a useful computational tool to study the properties of classical and quantum inhomogeneous fluids, especially for large systems where the DF methods provides a good compromise between accuracy and computational cost. In particular, a quite accurate description of the $T=0$ properties of liquid ^{4}He has been obtained within a DF approach by using the energy functional proposed in Ref. 2 and later improved in Ref. 3. In general, the density functionals for ^{4}He depend on a number of phenomenological parameters which are adjusted to reproduce *bulk* experimental properties of liquid ^{4}He at saturated vapor pressure. The resulting functionals are found to describe accurately also the properties of the inhomogeneous systems (e.g., the liquid-vapor interface of the free ^{4}He surface) (for a thorough comparison between density functionals used to describe liquid ^{4}He at $T=0$, see Ref. 4).

The phenomenological density functional of Ref. 3 has been widely used in a variety of problems involving inhomogeneous ^{4}He systems like pure and doped clusters,[5–7] electron "bubbles" in bulk ^{4}He,[8] alkali atom adsorption on the surface of liquid ^{4}He,[9] vortices in ^{4}He clusters,[10] adsorption of liquid ^{4}He on solid surfaces,[11,12] etc.

According to Ref. 3 the static properties of liquid ^{4}He at $T=0$ are described by the following energy density functional (atomic units will be used throughout our paper):

$$E_0[\rho]=\frac{1}{2M}\int d\mathbf{r}(\nabla\sqrt{\rho})^2+\frac{1}{2}\int d\mathbf{r}\int d\mathbf{r}'\rho(\mathbf{r})\rho(\mathbf{r}') \times V_{\text{He-He}}(|\mathbf{r}-\mathbf{r}'|)+\int d\mathbf{r}\ \ E_c(\mathbf{r}). \tag{1}$$

The first term on the right hand side is the quantum pressure (corresponding to the kinetic energy of a Bose gas of nonuniform density). The second term contains a two-body pair potential $V_{\text{He-He}}$ screened at short distances, while the last term accounts for correlation effects due to the short-range part of the He-He interaction. The explicit form of the functional (1) is given in Ref. 3, to which the reader is referred for more details (see also the Appendix in the present paper).

The minimization of the energy functional (1) with respect to density variations, subject to the constraint of a constant number of ^{4}He atoms $\int\rho(\mathbf{r})d\mathbf{r}=N$, leads to the equilibrium profile $\rho(\mathbf{r})$, thus allowing to study the *static* properties of the ^{4}He system.

In order to study the *dynamics* of ^{4}He an additional term [which has no effect on the static properties derived from the minimization of the energy functional (1)] has been added[3] to the functional (1) in the form of a phenomenological current term

$$H_J[\rho,\mathbf{v}]=\frac{\rho(\mathbf{r})}{2}M\mathbf{v}(\mathbf{r})^2-\frac{M}{4}\int d\mathbf{r}'V_J(|\mathbf{r}-\mathbf{r}'|) \times\rho(\mathbf{r})\rho(\mathbf{r}')[\mathbf{v}(\mathbf{r})-\mathbf{v}(\mathbf{r}')]^2. \tag{2}$$

The first term is the usual hydrodynamic current density, while the second term accounts in a phenomenological way for nonlocal effects due to the "backflow" current density.[3] The resulting DF (the so-called Orsay-Trento functional), which will be used in our calculations, has thus the following form:

$$E[\rho,\mathbf{v}]=E_0[\rho]+\int d\mathbf{r}\ \ H_J[\rho,\mathbf{v}]. \tag{3}$$

An important feature of the above functional, which will prove to be essential in the time-dependent calculations presented in the following sections, is that it is explicitly designed to reproduces not only the static structure factor but also the bulk dispersion relations of sound excitations in liquid ^{4}He and the dynamic structure function as well, i.e., the effective current-current interaction V_J in H_J is empirically chosen in such a way that the dispersion relation for bulk ^{4}He derived from Eq. (3) exactly matches the experimental phonon-roton spectrum of ^{4}He.

The extended functional (3) has been applied in the past to the study of density oscillations in ^{4}He clusters,[13] of surface excitations in ^{4}He films,[3,5] and of other related dynamical phenomena.[14] In all of the above applications a linear

response approximation was used, as well as suitable symmetries were assumed in order to make the calculations feasible.

There are many different situations, however, where a more general approach to investigate the microscopic dynamics of liquid ^{4}He in arbitrary environments, often characterized by geometrical confinement, is highly desirable. For instance, modifications of the excitation spectra due to geometrical confinement are expected in the case of ^{4}He films adsorbed on solid surfaces. A second example involves impurity-doped ^{4}He clusters. Atomic impurities are currently used as experimental probes of the superconducting behavior of ^{4}He clusters: the coupling of the impurity motion with the cluster dynamics is crucial for a comprehension of the observed spectra. As a third example, we mention the problem of the dynamics of wetting phenomena: weakly attractive surfaces such as the heavy alkali metal surfaces are not wet by liquid ^{4}He at very low temperature, and thus a finite amount of ^{4}He on these surfaces will form a droplet characterized by a nonzero contact angle. Even on a highly uniform surface, however, the contact angle between the ^{4}He droplet and the surface is extremely hysteretic and its value strongly depends on whether the contact line is advancing or receding. Informations from microscopic calculations of the dynamic behavior of a liquid droplet/film spreading on a weak solid surface can represent a valuable help to understand these effects.

We present here calculations, done in the framework of time-dependent density functional (TD-DFT) phenomenological theory, of the dynamical properties of ^{4}He (at $T=0$) in confined geometries. Our methods allows to calculate the direct real-time evolution of a ^{4}He system in arbitrary three-dimensional geometries. Some applications of the method, showing its efficiency and capabilities, will be presented in the following sections.

II. TIME-DEPENDENT DENSITY FUNCTIONAL THEORY

In order to extend the DFT scheme described in the previous section to the domain of time evolution (TD-DFT), one can use a variational principle as follows. One starts from a suitable action integral A written in terms of a complex "wave function" $\Psi(\mathbf{r},t)$

$$A[\Psi]=\int dtd\mathbf{r}\left\{\mathcal{E}[\Psi,\Psi^*]-i\Psi^*\frac{\partial\Psi}{\partial t}\right\}, \tag{4}$$

where the energy density $\mathcal{E}$ is defined by $\int d\mathbf{r}\mathcal{E}=E[\rho,\mathbf{v}]$. From the condition of stationarity

$$\frac{\delta A}{\delta\Psi^*}=0 \tag{5}$$

a time-dependent Euler-Lagrange equation follows:

$$\left[-\frac{\nabla^2}{2M}+U[\rho,\mathbf{v}]\right]\Psi\equiv H\Psi=i\frac{\partial\Psi}{\partial t}. \tag{6}$$

The "effective potential" U appearing in the above nonlinear time-dependent Schrodinger equation is defined as the variational derivative of the energy functional, $U[\rho,\mathbf{v}]\equiv\delta E[\rho(\mathbf{r})]/\delta\Psi^*$ and its explicit expression is given in the Appendix. From the solution $\Psi\equiv\phi e^{i\Theta}$ of Eq. (6) one can get the time-dependent density $\rho(\mathbf{r},t)=\phi^2$ and the fluid velocity field $\mathbf{v}(\mathbf{r},t)=(1/M)\nabla\Theta$. We describe in the following section the numerical procedure that we used in order to integrate numerically the Eq. (6).[15,16]

III. COMPUTATIONAL SCHEME

The numerical solution of Eq. (6), i.e., the wave function at an arbitrary time t, $\Psi(\mathbf{r},t)$, is obtained by using the Crank-Nicholson's (CN) scheme, which enables to evolve $\Psi(t)$ to a later time $t+\Delta t$:

$$\left[1+i\frac{\Delta t}{2}H(t+\Delta t)\right]\Psi(t+\Delta t)=\left[1-i\frac{\Delta t}{2}H(t)\right]\Psi(t). \tag{7}$$

The CN algorithm is one of the many approximate methods that can be used to integrate numerically a time-dependent Schrödinger equation such as the one shown in Eq. (6). It is second order accurate in Δt, as can be easily seen by expanding the two sides of Eq. (7) in powers of Δt. Among the advantages of such scheme is its numerical stability for long-time evolutions, and the unitariness (i.e., the number of particles is conserved during the time evolution).[17] The CN recursion can be easily solved iteratively for each time step evolution. We find that three iterations are usually enough to guarantee a stable evolution even during long simulation times.

The application of the CN formula requires the calculation of the action of the "Hamiltonian" $H\equiv-(1/2M)\nabla^2+U[\rho,\mathbf{v}]$ to the complex wave function Ψ. In order to calculate efficiently the convolution integrals of the form $I(\mathbf{r})=\int d\mathbf{r}'f(\mathbf{r}-\mathbf{r}')g(\mathbf{r}')$ appearing in the potential term U (whose explicit expression is reported in the Appendix) we employ a Fourier representation of the basic quantities Ψ and of the density ρ. Since the Fourier transform of a convolution is the product of the Fourier transforms of the two terms entering the integrals, one can perform efficiently the calculations of such convolution integrals on a computer by using fast Fourier transforms (FFT).

The use of FFT implies periodic boundary conditions (PBC's), and thus our calculations have been performed using a periodically repeated supercell containing N Helium atoms. Both Ψ and ρ are expanded in plane waves: $\Psi(\mathbf{r})=\Sigma_{\mathbf{G}}\Psi_{\mathbf{G}}e^{i\mathbf{G}\cdot\mathbf{r}}$, and similarly for ρ. The $\mathbf{G}$'s are the supercell wave vectors, $\mathbf{G}=\pi(n/L_x,m/L_y,p/L_z)$, with $n,m,p=0,\pm1,\pm2,\ldots,$ and L_x,L_y,L_z are the sides of the supercell (a primitive orthorhombic supercell is used in all our calculations). The number of plane waves in the above expansions is chosen such as to give converged values for the total energy E and for the structural parameters of the ^{4}He system under investigation. In the various applications that we report in the following, the supercell size was always chosen in such a way to make negligible the interaction of the ^{4}He system with its repeated images.

The action of the kinetic energy operator $\hat{T} \equiv -(1/2M)\nabla^2$ on the wave function Ψ is also evaluated in reciprocal space, i.e.,

$$\hat{T}\Psi = \frac{1}{2M} FFT\{G^2 \Psi_G\}. \tag{8}$$

Finally, the real-space expression of $H\Psi$, computed as described above, is used in the iteration formula of the CN scheme to give the evolved wave function $\Psi(t+\Delta t)$. A new potential U is thus computed from the updated density and velocity, and the procedure is repeated for the next time step. Typical time steps Δt which are found to give stable time evolutions are of the order of 1–3 fs.

We stress the fact that no geometric or symmetry constraints are imposed during the time evolution to reduce the computational effort. Our computational scheme is thus general and can be applied in particular to those situations characterized by geometrical confinement of ^{4}He. We will give in the following sections few examples of such case.

IV. ^{4}He BULK EXCITATIONS

One important feature of the most recent implementation of DF for ^{4}He used here is the inclusion of a ''backflow'' current term [the second term in Eq. (2)] explicitly depending on the fluid velocity as well as on the fluid density, such that the resulting functional is able to correctly reproduce the bulk excitation spectrum of liquid ^{4}He. This can be immediately verified within our computational scheme as follows.

We setup an initial state corresponding to a modulation of the bulk uniform density with a wave vector **q**:

$$\Psi(\mathbf{r}, t=0) = \{\rho_0[1+\epsilon \sin(\mathbf{q}\cdot\mathbf{r})]\}^{1/2}, \tag{9}$$

where ϵ is a small amplitude and $\rho_0 = 0.02184$ Å^{-3} is the saturation density at zero temperature and pressure. The system is then allowed to evolve in time according to the CN scheme described above. By monitoring the periodic oscillations of $\rho(\mathbf{r},t)$ during the simulation, we can immediately calculate the mode frequency

$$\omega = \frac{2\pi}{T} = \omega(\mathbf{q}). \tag{10}$$

Here T is the period of the observed oscillation. By varying the wave vector **q** we get the whole dispersion curve of ^{4}He, which we compare in Fig. 1 with the experimental data. As it appears from Fig. 1, the agreement with the measured data is very good in a wide range of values of the wave vector **q**.

We finally note that if the bulk dispersion relation is calculated by neglecting the ''backflow'' term in Eq. (2), results deviating by as much as 50% from the experimental curve are obtained for $q > 0.5$ Å^{-1}.

V. DYNAMICS OF ^{4}He CLUSTERS

The dynamics of liquid ^{4}He clusters have been studied theoretically in recent years by means of a number of different methods and thus represents a convenient benchmark for our numerical scheme. We have considered the *monopole*

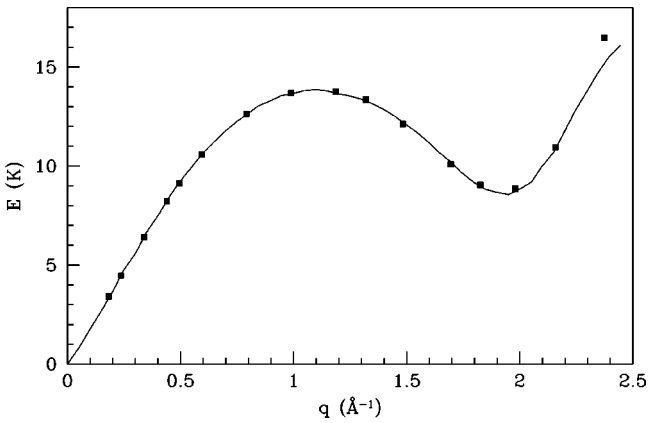

FIG. 1. Bulk ^{4}He excitation spectrum. The points show the calculated spectrum, while the solid line shows the experimental dispersion relation.

and *quadrupole* vibrational modes of cluster of different sizes, characterized by the angular momentum quantum number $l=0$ and $l=2$, respectively. The dipole mode ($l=1$) corresponds to a translation of the cluster as a whole, and should thus lie at zero energy. To study the monopole mode, which is a radial breathing oscillation of the cluster density, we compute the main frequencies by monitoring the periodic variations with time of the mean square radius of the cluster

$$R(t) = \sqrt{\frac{1}{N}\int r^2 \rho(\mathbf{r},t)\, d\mathbf{r}}. \tag{11}$$

To study the quadrupole oscillations we analyze instead the time evolution of the quadrupole moment tensor Q_{ij}:

$$Q_{ij}(t) = \int \rho(\mathbf{r},t)[3r_i r_j - r^2\delta_{ij}]\, d^3r. \tag{12}$$

Suitable initial states for both modes are constructed by applying to the ground state wave function $\Psi_0 = \sqrt{\rho_{\rm eq}}$ [where $\rho_{\rm eq}$ represents the equilibrium density profile for the cluster, calculated as described in Sec. I by direct minimization of the energy functional (1)] an excitation operator $e^{i\xi F}$, where $F = r^2$ to excite monopole oscillations, while $F = r^2 Y_{20}$ to excite quadrupole oscillations

$$\Psi(\mathbf{r}, t=0) = e^{i\xi F}\Psi_0(\mathbf{r}). \tag{13}$$

This initial state is thus allowed to evolve according to Eq. (6). From a frequency analysis of the calculated $M(t)$ and of $Q_{ij}(t)$ we then calculate both the amplitudes and the frequencies of the observed oscillations.

We report in Fig. 2 the calculated frequencies of the main oscillations observed in the discrete region of the spectrum (i.e., below the evaporation threshold $\omega < |\mu|$, μ being the chemical potential of a single ^{4}He atom).

For comparison, we show in the same figure the results taken from Ref. 18, obtained within the random phase approximation (RPA) and using a zero-range density functional to describe the ^{4}He system. The approach used in Ref. 18, which neglects completely the short-range He-He correlation

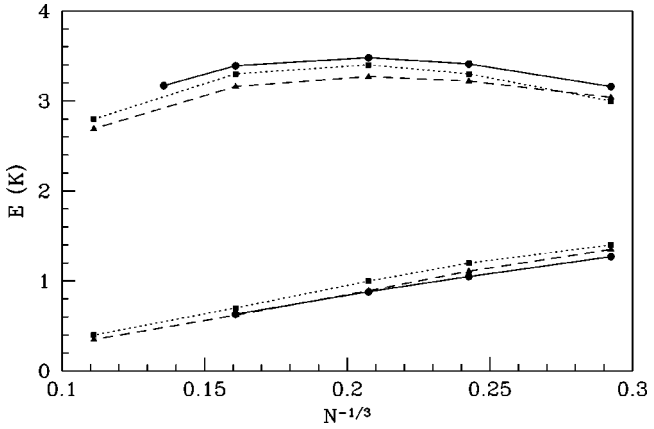

FIG. 2. Calculated monopole (upper lines) and quadrupole (lower lines) oscillation frequencies of liquid ^{4}He clusters, shown as a function of the cluster sizes. Dots: this work; squares: results from Ref. 18; triangles: results from Ref. 6.

effects, is accurate only when applied to the study of excitations involving variations in space larger than the average distance between the ^{4}He atoms: this is not, however, a major limitation for the long-wavelength modes like the ones investigated here [external field proportional to $r^l Y_{l0}(\hat{\mathbf{r}})$].

In the same plot we compare also our calculated frequencies with those obtained from more recent calculations done by using a finite-range DF including nonlocal effects, very similar to the one used here, and again within RPA.[6] The results are not much different from those obtained using a zero-range functional,[18] showing that the effects of nonlocalities are not important in this case due to the $q\sim 0$ character of the multipole excitations studied here.

Our calculated values, as it appears from Fig. 2, do not differ much from the two previous theoretical results, even if they are obtained by explicitly including the ''backflow'' term [see Eq. (2)] in the ^{4}He density functional. The reason is that this term becomes important in the region where the bulk dispersion relation deviates from its phononlike behavior, whereas in the present case only low-q excitations are considered. In the next sections we will present cases where the inclusion of the backflow term is instead crucial in order to get accurate results.

VI. EXCITATIONS OF A ^{4}He MONOLAYER ADSORBED ON A WEAKLY ATTRACTIVE SURFACE

The study of the structure, growth and excitations of liquid ^{4}He films adsorbed on solid surfaces is an important field of current research on superfluid properties. Reliable theories of inhomogeneous liquid ^{4}He may represent a useful complementary tool for studying the properties of liquid ^{4}He interacting with a solid surface.[19]

Because of the extremely weak He-He interaction, liquid ^{4}He in contact with almost any substrate spreads to form a continuous film over the surface, so that vapor and substrate are never in contact. A remarkable exception to this behavior is found when ^{4}He is adsorbed on heavy alkali metal surfaces: due to the large electron spill-out at these surfaces, alkali metals provide the weakest adsorption potentials in nature for He atoms. Based on this observation, it was suggested[20,21] that ^{4}He might not wet some heavy alkali metal surfaces. Subsequent experiments have confirmed this remarkable prediction.[22–25]

We study here the excitations of a single *monolayer* of liquid ^{4}He, adsorbed on a weakly attractive surface. We choose here the surface of Rb: this is because Rb is the weakest surface that it is actually wet by ^{4}He at $T\sim 0$, i.e., the stable state of a finite amount of liquid^{4}He on Rb is represented by a thin liquid film covering the whole surface, rather than being represented by a droplet as in the case of Cs. The extremely weak He-surface interaction on the other hand is expected to act as a small perturbation on the film. Thus the excitations studied here should be representative to some extent of those for an isolated ^{4}He film (note, however, that a truly free, unsupported planar ^{4}He film is actually always unstable[26,27]).

To model the interaction with a Rb substrate, we use a binding potential $V_s(z)$ which describes the interaction between Rb, occupying the half space $z\leqslant 0$, and one ^{4}He atom located at a distance z above the surface, which is taken to be ideally flat. The explicit form for $V_s(z)$, originally proposed in Ref. 28, was later revised in Ref. 12 in order to correctly reproduce the experimental wetting properties of the ^{4}He/Rb system, i.e., complete wetting at $T\sim 0$. We do not include any corrugation of the surface on the atomic scale to mimic its actual microscopic structure. This is a good approximation for the case of ^{4}He adsorption on alkali metal surfaces, because the experiments[29] indeed indicate that a surprisingly smooth surface is seen by adsorbed ^{4}He atoms.

The total energy functional of liquid ^{4}He interacting with a Rb surface is thus described by the energy functional (3) augmented by the additional term $\int d\mathbf{r}\rho(\mathbf{r})V_s(z)$, which describes the interaction energy due to the presence of the surface. We have preliminarily studied the equilibrium density of liquid ^{4}He on the Rb surface, at different areal coverages. Our results are reported in Fig. 3, where the density profiles in the direction perpendicular to the surface (which is located at $z=0$) are shown. Note that as the coverage increases, a second layer starts to form above the first layer. Quite arbitrarily, we take as representative of a ''monolayer'' the profile shown in Fig. 3 with a thicker line, corresponding to $n=4.2\times 10^{-2}$ Å^{-2}.

We thus prepare our monolayer in a suitable nonequilibrium initial state, characterized by a density modulation with a wave vector $\mathbf{q}$ parallel to the surface. We note that, due to the presence of a symmetry-breaking external potential (the He-surface potential) which depends on z (the coordinate normal to the surface), such initial state will be immediately coupled, during its time-evolution, to excitations of the film polarized perpendicularly to the surface plane.

From a Fourier analysis of the density variations during the time evolution from this initial state, we are able to get the main excitations of the ^{4}He film. Figure 4 shows our results. The filled and empty squares show the main features observed in the frequency spectrum of the time-dependent density $\rho(\mathbf{r},t)$. The filled squares indicate the most intense peaks, whereas the open squares indicate the somewhat

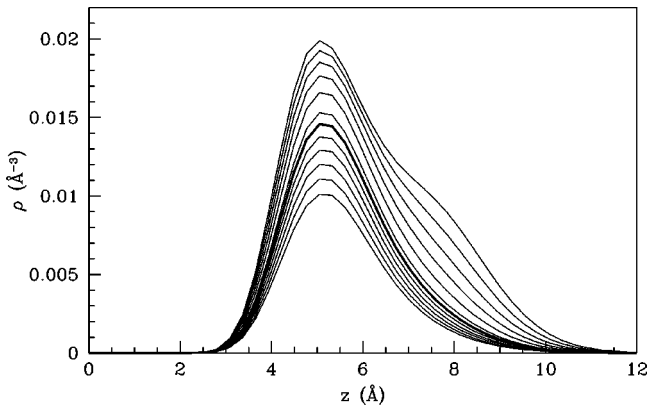

FIG. 3. Equilibrium density profiles for ^{4}He films adsorbed on a Rb surface. The z direction is perpendicular to the surface plane. Different curves represent increasing values of the surface coverages (number of ^{4}He atoms per unit surface area), from $n=1.6\times10^{-2}$ Å^{-2} (lower profile) to $n=7.2\times10^{-2}$ Å^{-2} (upper profile). The thicker line (defining our ''monolayer'') is drawn at $n=4.2\times10^{-2}$ Å^{-2}.

weaker features in the spectrum.

At low values of the wave vector q the modes of a thin^{4}He film adsorbed on a solid surface will be a combination of both ''shallow'' third sound waves, characterized by a linear dispersion $\omega\sim c_3 q$, and ''shallow'' capillary waves (analogous to the ''ripplons'' excitations on the ^{4}He surface), characterized by a quadratic dispersion $\omega\sim q^2$.

The former modes are driven by the He-surface interaction potential (the third sound velocity c_3 being proportional to the Van der Waals coefficient in the long-range part of the He-surface potential). The latter modes,[31] which are driven solely by the ^{4}He surface tension, are ''ripplonlike'' surface excitations modified by the finite thickness of the film in such a way that the resulting dispersion relation is (in the low-q limit)

$$\omega(q)\sim\omega_{\text{ripplon}}(q)(qd)^{1/2}. \tag{14}$$

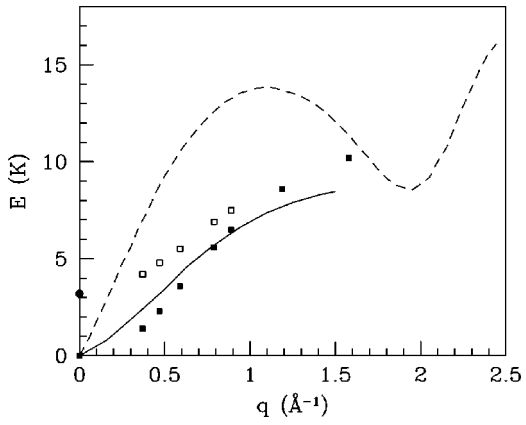

FIG. 4. Calculated dispersion curves for a ^{4}He monolayer adsorbed on a Rb surface (squares). The dashed line is the bulk dispersion relation, while the solid line shows the experimental ''ripplon'' dispersion.

Here d is the thickness of the ^{4}He film. Since $\omega_{\text{ripplon}}\sim q^{3/2}$, a quadratic dispersion with q results.

By assuming that an hybrid dispersion relation which contains both types of excitations holds,[32] one finds that the crossing between the two dispersion curves occurs at $q_c=(Mc_3^2\rho_0/\sigma d)^{1/2}$. Here M is the ^{4}He mass, ρ_0 is the saturation density at zero temperature and pressure and $\sigma=0.38$ erg/cm^2 is the He surface tension. For $q>q_c$ the spectrum is dominated by the capillary waves, whereas for $q<q_c$ third sound dominates.

The third sound velocities c_3 calculated using the DF used in our calculations are characterized by an oscillatory behavior with the ^{4}He coverage and can be very small especially near monolayer completion.[3] In order to estimate q_c we assume $c_3\sim20$ m/s (see Fig. 16 of Ref. 3). For the film thickness we take, from Fig. 3, $d\sim2$ Å. We thus find $q_c\sim0.1$ Å^{-1}, i.e., the low-q dispersion relation should be dominated, in the range of q values covered by our calculations, by shallow capillary waves where $\omega\sim q^2$.

From our results reported in Fig. 4 (lower branch at low q) it appears that at low-q values the lower dispersion curve becomes softer that the experimental ripplon curve[30] (shown for comparison with a solid line), being indeed consistent with the q^2 behavior discussed previously.

We cannot unfortunately verify the presence of a linear dispersion characteristic of third sound at very low q, because for very low excitation energies our method of extracting the frequencies ω becomes cumbersome and inaccurate (much longer simulation times, $t\gg1/\omega$, are needed).

Although a definite character cannot be assigned unambiguously to the observed mode shown in Fig. 4 due to the strong mixing between the two bands, we suggest that the upper branch should have a strong component of density modulations perpendicular to the surface. To verify this we have induced in the monolayer a simple $q=0$ mode where the ^{4}He film is initially rigidly shifted (by a very small amount) towards the surface. Due to the presence of the holding He-surface potential, the film once let free to evolve, executes a motion where it executes oscillations mainly perpendicular to the surface, with a main frequency at about 3 K: this value is shown with a filled dot at $q=0$ in Fig. 4.

We can compare our results for the film excitations with those obtained in Ref. 27 by means of a microscopic statistical theory, where the dynamic excitations of thick ^{4}He films on a Cs surface were considered. In that work it is found that ripplon modes appear in the calculated spectra, whose dispersion follows the $q^{3/2}$ law for surface excitations, as well as ''interfacial'' ripplons localized mainly at the ^{4}He/surface interface. In particular, the lowest mode calculated in Ref. 27 (corresponding the lower branch in Fig. 4) has a ripplon character. The second mode has a ''longitudinal'' character (i.e., parallel to the surface) on stronger substrates, only on very weak surfaces (i.e., Cs) it has a visible perpendicular component. A linear (third sound) dispersion has been also observed in Ref. 27 as long as the wavelength is large compared with the film thickness. We do not observe any such modes for the reasons outlined previously.

We believe that the upper branch in Fig. 4 is the counterpart of a similar excitations observed in neutron diffraction experiments on ^{4}He adsorbed on a graphite substrate,[33] where, among other excitations, almost dispersionless modes at low frequencies have been observed. These mode have been interpreted,[34] by means of microscopic calculations, as standing waves of the ^{4}He liquid perpendicular to the substrate. We cannot compare directly our results with the experimental measurements of Ref. 33 and with the microscopic calculations of Ref. 34 because of the different substrate used (graphite is a much ''stronger'' substrate than alkali metal surfaces) and because multilayer films were considered in these references. We hope that our results will stimulate further experimental measurements, in particular to study the excitations of ^{4}He monolayers on weakly attractive surfaces.

VII. DYNAMICS OF ALKALI-DOPED ^{4}He CLUSTERS

The spectroscopy of doped liquid ^{4}He clusters has become a current tool for the study of superfluidity in ^{4}He droplets.[35] As a consequence of the ultraweak alkali-He interaction, an alkali atom picked up by a ^{4}He cluster has its stable state in a ''dimple'' on the surface of the cluster,[9,36] rather than being solvated into its interior similar to most of the other atomic impurities. Thus alkali could provide an excellent probe for the *surface* excitation of superfluid nanodroplets.[36] The analysis and interpretation of experimental studies of the formation of ^{4}He-alkali complexes in doped clusters would thus benefit from theoretical work of the excitations of impurities attached to ^{4}He clusters.

Although for light alkali the motion of the impurity can be considered to a first approximation as occurring in a *static* ^{4}He environment (i.e., He does not adjust appreciably to the instantaneous atom position), however, for heavy alkali (Rb,Cs) a full dynamical approach is required, where the ^{4}He atoms in the cluster are allowed to adjust dynamically upon the motion of the adsorbed impurity.

We address here the problem of finding the spectrum of vibrational excitations of a ''dimple'' state. We consider in particular the system composed of a single Rb atom (in its electronic ground-state) attached to a 300-atom ^{4}He cluster. The Rb-He interaction is taken from Ref. 37.

Figure 5 shows the calculated equilibrium density profile (in a plane containing the center of the cluster and the Rb atom) for the ''dimple'' state representing the lowest energy configuration of the Rb$-^4$He system. By applying to the Rb atom a small initial momentum towards the surface of the cluster, we observe that the impurity starts oscillating around its equilibrium position shown in Fig. 5, and at the same time the ^{4}He density changes in time to adjust dynamically to the instantaneous Rb position. Our results for the Rb dynamics are shown in Fig. 6. In the upper panel we show the calculated instantaneous position of the Rb atom as a function of time (measured with respect to the Rb-cluster center-of-mass). A straightforward Fourier transform of the signal shown in the upper panel allows to compute the frequency spectrum shown in the lower panel.

We compare our results with a previous estimate[38] based on *static* DF calculations, where the frequency of the oscillations of a Rb atom attached to a 300-atom cluster was estimated approximately by assuming that the He atoms adiabatically adjust to the instantaneous position of the impurity. In that case the value of the frequency was extracted

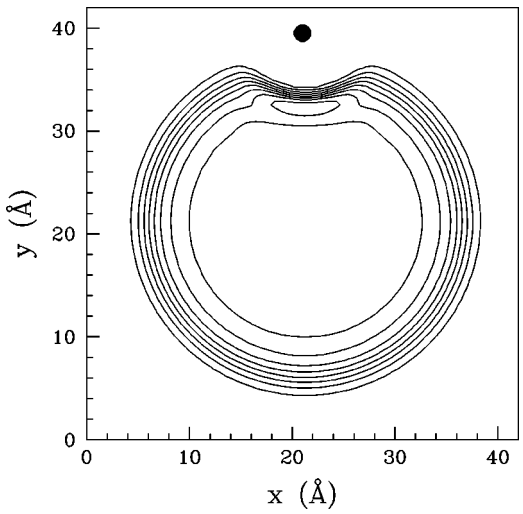

FIG. 5. Density contour plot for a 300-atom ^{4}He cluster with a Rb atom attached on its surface: the dot shows the equilibrium position of the Rb impurity.

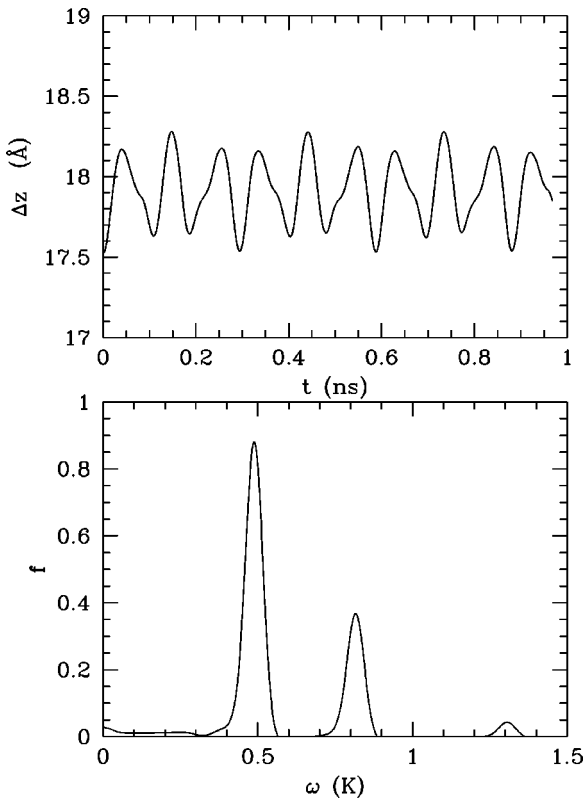

FIG. 6. Upper panel: Rb displacement with respect to the center-of mass of the Rb-cluster system, measured along the radial direction, as a function of the simulation time. Lower panel: Fourier spectrum (in arbitrary units) of the time series shown in the upper panel.

from the shape of the impurity-He potential energy surface, giving $\omega \sim 0.7$ K. It appears from our results that a more complex dynamics occurs, due to the coupling of the Rb atom motion with the surface oscillations of the cluster. The frequency of a surface mode of an N-atom ^{4}He cluster can be written as $\omega = \sqrt{l(l-1)(l+2)}\,\omega_0/\sqrt{N}$ where $\omega_0 = 3.45$ K. This is approximately ~ 0.6 K for the lowest $l = 2$ mode, i.e., close to the natural Rb frequency calculated in Ref. 38. A large amount of mixing is thus expected, which determines the appearance of the complex vibrational spectrum shown in Fig. 6.

Experimental measurements of such oscillations are under way[39] to confirm our predictions. A more complex and challenging application of time-dependent methods, i.e., the study of the oscillations of an alkali impurity in an *excited* electronic state, is currently in progress.

VIII. SPREADING OF A ^{4}He NANODROPLET ON A WEAKLY ATTRACTIVE SUBSTRATE

The mechanism underlying the spreading of a liquid droplet on a solid substrate is a long-standing problem. Experiments done on a number of different (classical) molecular fluids have revealed universal laws such as the Tanner' spreading law,[40] where the droplet radius grows as $r(t) \propto t^{1/10}$, as well as fascinating phenomena on the atomistic scale (such as the appearance of a monolayer film advancing in front of the drop,[41] two different regimes of the growth of the radius with time,[42] dynamical ''layering,'' etc.). Other experiments[41] have shown that one or more monomolecular precursor layers spread ahead of the droplet cap with an average radius $R(t) \sim \sqrt{t}$.

Numerical studies of droplet spreading have been performed[42–45] in recent years. Despite many efforts, however, many microscopic details of the spreading process are, however, still to be known.

Even more challenging is the behavior of a superfluid ^{4}He droplet on a weakly attractive surface: it has been found that ^{4}He droplets adsorbed on a Cs substrate have spreading and flow properties that are not simple consequences of bulk superfluid behavior.[46] When a ^{4}He droplet is deposited on a Cs surface (the only material known that is not wet by superfluid ^{4}He at very low temperature), even on a highly uniform surface the contact angle between the droplet and the surface is extremely hysteretic and its value strongly depends on whether the contact line is advancing or receding. Superfluid ^{4}He droplets on Cs are also remarkable because they can resist flow against a substantial chemical potential gradient.[46]

We have studied the spreading of a 200-atom He cluster on a weakly attractive surface. We choose for the latter the case of Cs (but very similar results are obtained for a Rb surface). To simulate the Cs surface, we use the ''*ab initio*'' potential developed in Ref. 28, which has applied successfully to the wetting properties of ^{4}He an a Cs surface.[12] The initial state is represented by a spherical cluster [whose density profile is obtained by minimization of the static functional (2) in the absence of the attractive He-surface potential], placed in the vicinity of the surface. The downward force responsible for the spreading of the droplet is provided solely by the long-range Van der Waals forces exerted by the substrate (due to the microscopic size of the droplet, the effect of gravity on spreading is negligible).

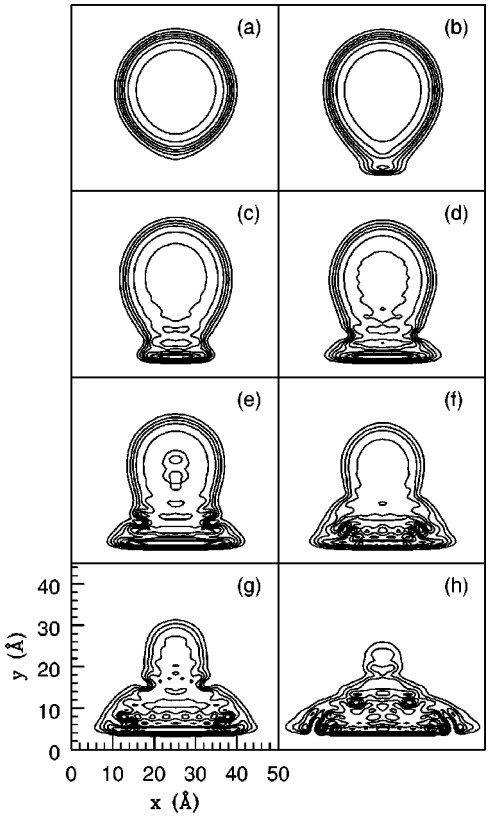

FIG. 7. Sequence of ^{4}He density contour plots showing the spreading of a 200-atom cluster on a Cs surface.

The spreading will continue, until the stable state is eventually reached. The nature of the latter depends on the strength of the He-surface potential: in the case of Cs, which is not wet by He at $T = 0$, the final configuration will be that of an almost spherical cap characterized by a contact angle of $\sim 40\,^\circ$ (partial wetting behavior).[11,46] More attractive substrate, on the other hand, will eventually be covered by a uniform microscopic film (complete wetting behavior). Due to the finiteness of our systems and our use of periodic boundary conditions our simulations are necessarily interrupted when the droplet hits its repeated images and starts coalescing with them.

The sequence characterizing the spreading process is shown in Fig. 7. The overall duration of the simulation shown in the figure is about 2 ns. Interestingly enough, a precursor layer seems to form under the cap of the spreading cluster. We have computed from the cluster density profile $\rho(\mathbf{r},t)$ the average radius R of this precursor layer. The dependence of R from time, shown in Fig. 8, shows a ''fast'' regime where the precursor layer expands linearly in time, as found in similar simulations for classical fluids.[45] Subsequently a slowing down occurs, in correspondence of the formation of the second layer [see panel (f) in Fig. 7]. It seems that after a transient, an almost linear spreading occurs again, although with a somewhat lower velocity. From the linear portion of Fig. 8 we get a speed of about ~ 50 m/s,

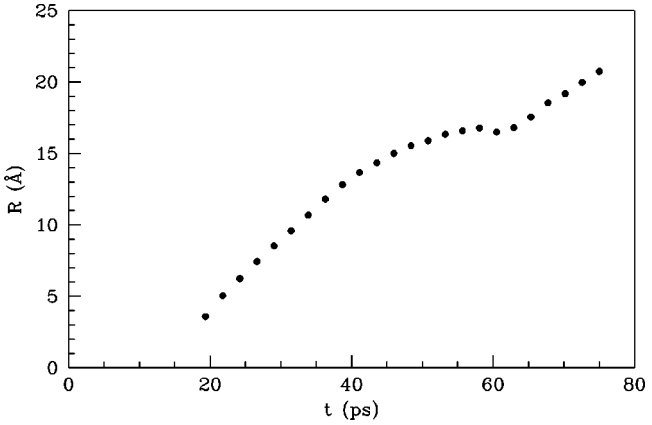

FIG. 8. Radius of the precursor layer as a function of time.

which is close to the critical Landau value. The slowing down is perhaps due to the spontaneous formation of vortical rings during the spreading. One such ring is shown in Fig. 9 by means of a vector plot showing the current density $\mathbf{J} \equiv \rho(\mathbf{r})\mathbf{v}(\mathbf{r})$ in a plane containing the center of the cluster and perpendicular to the Cs surface. Figure 9 also clearly shows the flow of atoms from the droplet cap feeding the underlying precursor film.

It is well known that a rotational (i.e., with $\nabla \times \mathbf{v} \neq 0$) motion of a quantum fluid described by a macroscopic wave function of the form $\Psi = \sqrt{\rho}\exp(i\Theta)$ can be realized only through the nucleation of vortex lines/rings. Along the core of the vortex the fluid density is zero and around it the circulation of the velocity field is quantized in units of h/M.

We have calculated the circulation of the velocity field associated with the vortex structure shown in Fig. 9 along a path enclosing the vortex core, but we did not find a quantized value for it. Moreover, the value of the circulation depends on the path chosen to calculate it. This is not due to a fault in the density functional used in our calculations. Rather, it has to be ascribed to the fact that the vortex ring in Fig. 9 is not really isolated: entangled with its own velocity field there is a complex flow of He atoms (from the cap to the precursor layer, and near the surface due to the expansions of the precursor layer itself) reflecting the spreading of the droplet.

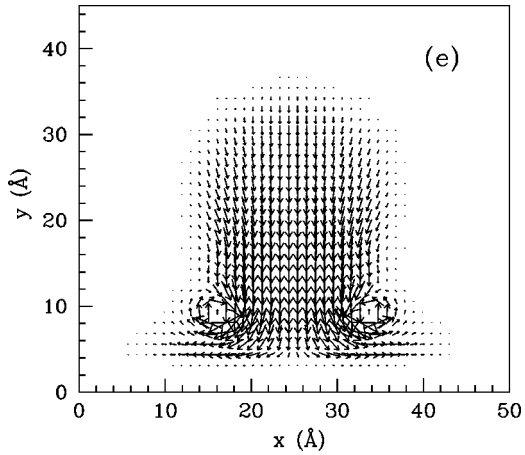

FIG. 9. Vector plot of the current density $\rho\mathbf{v}$ in a plane perpendicular to the surface and passing through the center of the cluster. The configuration shown corresponds to the density contours in panel (e) of Fig. 7.

In fact it can be shown that in different situations, the DF used in our calculations is perfectly adequate to produce quantized vortex structures in liquid ^{4}He. For instance, in the case of a rotating He cluster, the minimization of the DF under suitable conditions results in the spontaneous formation of a linear vortex trapped in the center of the cluster, and the circulation of the resulting velocity field around the vortex core turns out to be almost perfectly quantized.[47]

Although transient precursor films spreading linearly with time have been obtained from MD simulations of classical fluids,[43,45] they have not been seen in any experiment. This is probably due to the fact that they represent the very early stage of the spreading process: as the equilibrium shape of the droplet is reached, the initial fast spreading is found to slow down to a power law $R(t) \sim t^{1/7}$,[48] when a regime dominated by dissipation due to the viscous flow starts to dominate. It would be extremely interesting to study how this slowing down (which is only suggested from our short-time results in Fig. 8) occurs in the case of superfluid flow.

The presence of surface disorder is expected to alter the dynamics of liquid ^{4}He films spreading on a solid surface, because the three-phase contact line of the spreading film/droplet can easily be pinned to these defects, modifying the velocity of the contact line as it advances (or recedes) on the surface. We are currently investigating the effect of simple defects on the atomic-scale (adatoms or vacancies) on the droplet spreading process discussed above.

IX. SUMMARY

We have presented TD-DFT calculations of the dynamical properties of ^{4}He in situations characterized by geometrical confinement. We have shown the feasibility and efficiency of fully 3D TD-DFT calculations to study the dynamics of liquid He-4 in a number of representative situations: the dynamics of pure and alkali-doped ^{4}He clusters, the excitations of a liquid ^{4}He monolayer adsorbed on a weakly attractive surface and the dynamics of a ^{4}He nanodroplet spreading on a Cs surface.

ACKNOWLEDGMENTS

We thank M. Pi, M. Barranco, E. Krotscheck, W. Ernst, F. Dalfovo, V.A. Apkarian, and M.W. Cole for useful comments and discussions. We thank V.A. Apkarian for giving us a copy of Ref. 16 prior to publication. We acknowledge funding from MIUR-COFIN 2001.

APPENDIX

The effective potential entering Eq. (6) can be readily evaluated by functional differentiation of the energy functional (3) (see Ref. 3 for its detailed expression):

$$U[\rho,\mathbf{v}]=V_s(\mathbf{r})+\int d\mathbf{r}'\rho(\mathbf{r}')V_l(|\mathbf{r}-\mathbf{r}'|)+\frac{c_2}{2}\overline{\rho}(\mathbf{r})^2$$
$$+\frac{c_3}{3}\overline{\rho}(\mathbf{r})^3+\int d\mathbf{r}'\rho(\mathbf{r}')[c_2\Pi_h(|\mathbf{r}-\mathbf{r}'|)\overline{\rho}(\mathbf{r}')$$
$$+c_3\Pi_h(|\mathbf{r}-\mathbf{r}'|)\overline{\rho}^2(\mathbf{r}')]+\frac{\alpha_s}{2M}\left(1-\frac{\rho(\mathbf{r})}{\rho_0}\right)\int d\mathbf{r}'$$
$$\times\left(1-\frac{\rho(\mathbf{r}')}{\rho_0}\right)\nabla_{r'}\rho(\mathbf{r}')\cdot\nabla_r F(|\mathbf{r}'-\mathbf{r}|)$$
$$-\frac{M}{2}\int d\mathbf{r}'V_J(|\mathbf{r}-\mathbf{r}'|)\rho(\mathbf{r}',t)[v(\mathbf{r})-v(\mathbf{r}')]^2$$
$$+\frac{i}{2\rho(\mathbf{r})}\nabla\cdot\int d\mathbf{r}'\cdot\mathbf{g}(\mathbf{r},\mathbf{r}'). \quad \text{(A1)}$$

$V_s(\mathbf{r})$ represents an additional external potential acting on the ^{4}He system. The second term contains a two-body ^{4}He$-^4$He pair potential $V_l(r)$ screened at distances shorter than a characteristic length h_l, while the third and the fourth term (correlation terms), which contains the average of the density over a sphere of radius h_l, $\overline{\rho}_r$, accounts for the internal kinetic energy and for the increasing contribution of the hard-core He-He repulsion when the density is increased. The last two terms represent the contribution to the potential U of the ''backflow'' term (2) introduced in Ref. 3 in order to reproduce the bulk excitation spectrum of liquid ^{4}He. In particular, the last term contains the ''backflow'' current $\mathbf{J}_B \equiv \int d\mathbf{r}'\cdot\mathbf{g}(\mathbf{r},\mathbf{r}')=\int d\mathbf{r}'V_J(|\mathbf{r}-\mathbf{r}'|)\rho(\mathbf{r})\rho(\mathbf{r}')[\mathbf{v}(\mathbf{r})-\mathbf{v}(\mathbf{r}')]$.

The free parameters h_l, c_2, c_3, α_s are adjusted in order to reproduce a number of experimental properties of *bulk* liquid ^{4}He. For a detailed description of the various terms and the numerical values of the adjustable parameters, we refer the interested reader to Ref. 3.

[1] R. Evans, Adv. Phys. **28**, 144 (1979).
[2] J. Dupont-Roc, M. Himbert, N. Pavloff, and J. Treiner, J. Low Temp. Phys. **81**, 31 (1990).
[3] F. Dalfovo, A. Lastri, L. Pricaupenko, S. Stringari, and J. Treiner, Phys. Rev. B **52**, 1193 (1995).
[4] L. Szybisz, Eur. Phys. J. B **14**, 733 (2000).
[5] F. Dalfovo, Z. Phys. D: At., Mol. Clusters **29**, 61 (1994).
[6] M. Barranco and E.S. Hernandez, Phys. Rev. B **49**, 12 078 (1994).
[7] F. Dalfovo, Phys. Rev. B **46**, 5482 (1992).
[8] F. Ancilotto and F. Toigo, Phys. Rev. B **50**, 12 820 (1994).
[9] F. Ancilotto, E. Cheng, M.W. Cole, and F. Toigo, Z. Phys. B: Condens. Matter **98**, 323 (1995).
[10] F. Dalfovo, R. Mayol, M. Pi, and M. Barranco, Phys. Rev. Lett. **85**, 1028 (2000).
[11] F. Ancilotto, A.M. Sartori, and F. Toigo, Phys. Rev. B **58**, 5085 (1998).
[12] F. Ancilotto, F. Faccin, and F. Toigo, Phys. Rev. B **62**, 17 035 (2000).
[13] M. Casas, F. Dalfovo, A. Lastri, Ll. Serra, and S. Stringari, Z. Phys. D: At., Mol. Clusters **35**, 67 (1995).
[14] F. Dalfovo, A. Franchetti, A. Lastri, L. Pitaevskii, and S. Stringari, Phys. Rev. Lett. **75**, 2510 (1995); J. Low Temp. Phys. **104**, 367 (1996).
[15] We are aware of another computational scheme for TD-DFT developed recently (Ref. 16) to solve Eq. (6), which has been used to study the dynamics of excess electron in liquid ^{4}He ''bubble'' states. At variance with the scheme proposed in Ref. 16, which is limited to radially symmetric dynamics, our implementation does not assume any symmetry in the system.
[16] J. Eloranta and V.A. Apkarian, J. Chem. Phys. (to be published).
[17] A. Askar and A.S. Cakmak, J. Chem. Phys. **68**, 2794 (1978).
[18] M. Casas and S. Stringari, J. Low Temp. Phys. **79**, 135 (1990).
[19] B.E. Clements, H. Forbert, E. Krotscheck, H.J. Lauter, M. Saarela, and C.J. Tymczak, Phys. Rev. B **50**, 6958 (1994).
[20] E. Cheng, M.W. Cole, W.F. Saam, and J. Treiner, Phys. Rev. Lett. **67**, 1007 (1991).
[21] E. Cheng, M.W. Cole, W.F. Saam, and J. Treiner, Phys. Rev. B **46**, 13 967 (1992).
[22] J.E. Rutledge and P. Taborek, Phys. Rev. Lett. **69**, 937 (1992).
[23] P.J. Nacher and J. Dupont-Roc, Phys. Rev. Lett. **67**, 2966 (1991).
[24] K.S. Ketola, S. Wang, and R.B. Hallock, Phys. Rev. Lett. **68**, 201 (1992).
[25] J. Klier, P. Stefanyi, and A.F.G. Wyatt, Phys. Rev. Lett. **75**, 3709 (1995).
[26] L. Szybisz, Phys. Rev. B **56**, 11 845 (1997).
[27] B.E. Clements, E. Krotscheck, and C.J. Tymczak, J. Low Temp. Phys. **107**, 387 (1997); B.E. Clements, E. Krotscheck, and M. Saarela, Z. Phys. B: Condens. Matter **94**, 115 (1994).
[28] A. Chizmeshya, M.W. Cole, and E. Zaremba, J. Low Temp. Phys. **110**, 677 (1998).
[29] J.D. White, J. Cui, M. Strauss, R.D. Diehl, F. Ancilotto, and F. Toigo, Surf. Sci. **307**, 1134 (1994).
[30] H.J. Lauter, H. Godfrin, V.L.P. Frank, and P. Leiderer, Phys. Rev. Lett. **68**, 2484 (1992).
[31] K.R. Atkins, Phys. Rev. **113**, 962 (1959); I.M. Khalatnikov, G.V. Kolmakov, and V.L. Pokrovsky, Sov. Phys. JETP **80**, 873 (1995).
[32] R.A. Guyer, M.D. Miller, and J. Yaple, Phys. Rev. B **25**, 4570 (1982).
[33] H.J. Lauter, H. Godfrin, and H. Wiechert, in *Proceedings of the Second International Conference on Phonon Physics*, edited by J. Kollar *et al.* (World Scientific, Singapore, 1985), p. 842.
[34] V. Apaja, H. Godfrin, E. Krotscheck, and H.J. Lauter, J. Low Temp. Phys. **124**, 599 (2001).
[35] J.P. Toennies and A.F. Vilesov, Annu. Rev. Phys. Chem. **49**, 1 (1998); K.K. Lehmann and G. Scoles, Science **279**, 2065 (1998).
[36] F. Stienkemeier, W.E. Ernst, J. Higgins, and G. Scoles, J. Chem. Phys. **102**, 615 (1995).
[37] S.H. Patil, J. Chem. Phys. **94**, 8089 (1991).
[38] F.R. Bruhl, R.A. Trasca, and W.E. Ernst, J. Chem. Phys. **115**, 10 220 (2001).
[39] W.E. Ernst (private communication).
[40] L.H. Tanner, J. Phys. D **12**, 1473 (1979).

[41] F. Heslot, A.M. Cazabat, and P. Levinson, Phys. Rev. Lett. **62**, 1286 (1989).
[42] J. De Coninck, U. d'Ortona, J. Koplik, and J.R. Banavar, Phys. Rev. Lett. **74**, 928 (1995).
[43] T.D. Blake, A. Clarke, J. De Coninck, M. de Ruijter, and M. Voue', Colloids Surf. **149**, 123 (1999).
[44] J. Yang, J. Koplik, and J.R. Banavar, Phys. Rev. Lett. **67**, 3539 (1991).
[45] J.A. Nieminen, D.B. Abraham, M. Kartunnen, and K. Kaski, Phys. Rev. Lett. **69**, 124 (1992).
[46] D. Ross, J.E. Rutledge, and P. Taborek, Science **278**, 664 (1997).
[47] F. Ancilotto, M. Pi, and M. Barranco (unpublished).
[48] M.J. de Ruijter, J. De Coninck, and G. Oshanin, Langmuir **15**, 2209 (1999).